doi:10.26443/seismica.v2i1.252

Estimates of earthquake temperature rise, frictional energy, and implications to earthquake energy budgets

G. L. Coffey * [1], **H. M. Savage** [2], **P. J. Polissar** [3]

[1]Department of Earth Structure and Processes, GNS Science, Lower Hutt, New Zealand, [2]Department of Earth and Planetary Science, University of California Santa Cruz, Santa Cruz, United States, [3]Department of Ocean Sciences, University of California Santa Cruz, Santa Cruz, United States

Author contributions: *Conceptualization*: G. Coffey, H. Savage. *Data Curation*: G. Coffey. *Formal Analysis*: G. Coffey. *Funding Acquisition*: G. Coffey, H. Savage, P. Polissar. *Investigation*: G. Coffey, H. Savage, P. Polissar. *Methodology*: G. Coffey, H. Savage, P. Polissar. *Project Administration*: G. Coffey. *Resources*: G. Coffey, H. Savage, P. Polissar. *Supervision*: H. Savage, P. Polissar. *Visualization*: G. Coffey, H. Savage. *Writing – original draft*: G. Coffey. *Writing – review & editing*: G. Coffey, H. Savage, P. Polissar.

Abstract Coseismic temperature rise is a fundamental state variable that changes dramatically during earthquakes due to frictional heating, however in situ temperatures are notoriously hard to measure. The development of multiple paleotemperature proxies over the last twenty years has led to an increasing number of coseismic temperature measurements collected across a variety of faults. Here we present the first compilation of coseismic temperature rise measurements and frictional energy estimates to investigate the contribution of frictional heating to the earthquake energy budget and how this varies over different fault and earthquake properties. This compilation demonstrates that coseismic temperature rise increases with the depth of faulting until ~5 km, and below this depth remains relatively constant. Frictional energy, similarly, increases with depth until ~5 km. However, frictional energy is remarkably similar across the faults studied here, with most falling below 45 MJ/m^2. Our results suggest that dynamic weakening mechanisms may limit frictional energy during coseismic slip. We also demonstrate a basic difference between small and large earthquakes by comparing frictional energy to other components of the earthquake energy budget. The energy budget for small earthquakes (<1-10 m of displacement) is dominated by frictional energy, while in large events (>1-10 m of displacement), frictional, radiated, and fracture energy contribute somewhat equally to the earthquake energy budget.

Production Editor:
Gareth Funning
Handling Editor:
Pathikrit Bhattacharya
Copy & Layout Editor:
Ethan Williams

Received:
October 10, 2022
Accepted:
May 16, 2023
Published:
June 5, 2023

Non-technical summary During an earthquake, frictional resistance can lead to generation of very high temperatures as both sides of the fault slide past each other rapidly. Understanding these temperatures and the energy that is dissipated as heat (the frictional energy) provides insight into how earthquakes start, propagate, and what leads to their arrest. Recently, more and more methods to address this have been developed, leading to a growing database of earthquake temperature measurements and frictional energy estimates. In this study we present the first compilation of these data. We find that earthquake temperature rise increases with the depth of faulting to ~5 km, and below this depth it remains fairly constant. We also find that frictional energy is remarkably similar across the faults studied here with most falling below 45 MJ/m^2 (for reference, 0.08 MJ is required to heat a single cup of coffee). This suggests that faults become very weak and slide more easily during earthquake slip, limiting the energy that is dissipated as heat. Our results demonstrate a basic difference between small earthquakes (<1-10 m of slip), where the earthquake energy budget is dominated by frictional heating, and large earthquakes (>1-10 m of slip) where energy is more equally split between frictional heating, radiating seismic waves, and damage (fractures).

1 Introduction

Temperature exerts a fundamental control on both the chemical and mechanical behavior of faults. During earthquakes, rapid frictional heating from fault slip can lead to a large increase in the in-situ near-fault temperature. These temperature spikes can have a profound effect on fault rheology, chemical disequilibria, and the rates of chemical reactions, leading to changes in fault strength, structure, and mineralogy (Reches and Lockner, 2010; Di Toro et al., 2011; Noda and Lapusta, 2013; Collettini et al., 2014). Although geologically brief, coseismic temperature rise is effectively a metamorphic process, however, very few observational estimates of coseismic temperature rise exist.

In addition to shedding light on chemo-mechanical processes during earthquakes, quantifying temperature rise during earthquake slip also allows us to place constraints on the earthquake energy budget. This is a key component in understanding earthquake physics as it controls a rupture's ability to grow and provides information on what processes facilitate rupture propagation or lead to its arrest. The earthquake energy budget comprises dissipative (frictional and fracture energy) and radiated energy (Figure 1; Kanamori and Heaton,

*Corresponding author: g.coffey@gns.cri.nz

2000). Portions of the earthquake budget that are related to stress drop can be measured or inferred from seismology, however the frictional energy depends on the absolute shear stress level during the earthquake. As seismology does not measure absolute stresses, we rely on measurements of coseismic temperature rise from frictional resistance to quantify frictional energy (Kanamori and Heaton, 2000). With the development of paleotemperature proxies and the installation of borehole observatories, a number of frictional energy estimates for different faults have been made (Pittarello et al., 2008; Fulton et al., 2013; Savage and Polissar, 2019; Coffey et al., 2021, 2022).

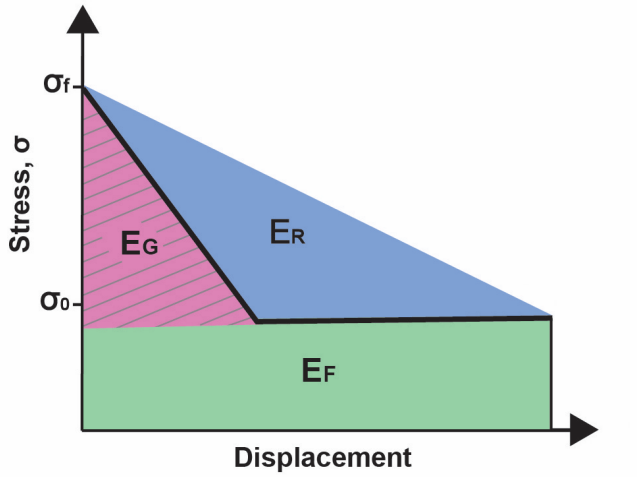

Figure 1 Simplified example of the earthquake energy budget based upon Kanamori and Heaton (2000) including frictional energy (E_F), fracture energy (E_G), and the energy radiated as seismic waves (E_R). The hatched area is the breakdown energy (Cocco and Tinti 2005), here it is depicted as equal to fracture energy, but it may also include frictional energy.

Here, we present a compilation of earthquake temperature and frictional energy estimates from a suite of fault types. The data are from a variety of paleotemperature proxies, but rely heavily on biomarker thermal maturity (Polissar et al., 2011; Savage et al., 2014; Sheppard et al., 2015; Savage and Polissar, 2019; Coffey et al., 2019; Rabinowitz et al., 2020; Coffey et al., 2021, 2022). This compilation is the first attempt to understand the frictional energy component of the earthquake energy budget from an observational perspective and enables exploration of how energy is partitioned into different sinks depending upon earthquake depth and other parameters.

2 Coseismic temperature rise and earthquake paleothermometry

During an earthquake, frictional resistance along a fault can lead to the generation of very high temperatures. The temperature rise (ΔT) that occurs during an event depends on various fault and earthquake properties:

$$\Delta T \propto \frac{\tau}{\rho c_p} \frac{vt}{2a} \tag{1}$$

where τ is shear stress (the product of normal stress and friction minus pore pressure), ρ is density, c_p is heat capacity, t is time, v is slip velocity, and a is the half width of the slipping layer. Equation 1 illustrates the essential parameters that relate temperature rise to faulting and earthquake slip. The absolute temperature rise is also influenced by heat diffusion away from the slipping surface (Lachenbruch, 1986) and the full equations that include heat diffusion can be found in Supplementary Material S1.

When solving Equation 1 for depths below a couple of kilometers and for pore pressures that follow an assumed regular hydrostat, heat generation for even moderate-size earthquakes can easily create temperatures that melt all or some of the minerals present. Evidence of this melt is preserved in the rock record as pseudotachylyte, crystallized frictional melt that has long been considered a robust recorder of coseismic slip (Sibson, 1973, 1975). However, pseudotachylyte is famously underrepresented in outcrop (Kirkpatrick et al., 2009) and absent on faults shallower than ~3 km depth (Sibson and Toy, 2006). This dearth of pseudotachylyte has been attributed to alternative dynamic-weakening mechanisms, such as thermal pressurization, that can make faults so weak during earthquakes that they did not achieve significant temperatures (Rice, 2006). Theoretical analyses of dynamic weakening have been supported by dozens of high-speed friction experiments, which demonstrated that faults weaken dramatically at fast slip rates (Di Toro et al., 2011). Although it is very likely that faults are weak during earthquakes, more recent studies have also suggested that evidence of pseudotachylyte can be difficult to observe in outcrop, especially when the pseudotachylyte itself has undergone retrograde reaction to other minerals (Kirkpatrick and Rowe, 2013). Whether faults lack pseudotachylyte or it is obscured in outcrop, it is clear that developing additional thermal proxies for faults would shed light on earthquake mechanics. Recently, a greater range of techniques has been applied to study coseismic temperature rise (Rowe and Griffith, 2015). In addition to pseudotachylyte these include thermal decomposition of calcite, vitrinite reflectance, (U-Th)/He of hematite and other minerals, and mineralogic/textural zoning (Pittarello et al., 2008; Sakaguchi et al., 2011a; Kirkpatrick et al., 2012; Collettini et al., 2013; Ault et al., 2015; Rowe and Griffith, 2015). For example, microstructural evidence of carbonate dissociation has been used to argue that temperatures greater than ~750 °C were achieved during earthquakes (Rodriguez-Navarro et al., 2009; Collettini et al., 2013). Vitrinite, a type of kerogen found in bituminous coal, has been widely applied in the hydrocarbon industry as its reflectance increases with increasing thermal maturity, which is a function of time and temperature. Vitrinite reflectance has also been shown to be sensitive to shorter, earthquake-duration heating and has been applied to quantify coseismic temperature rise in settings

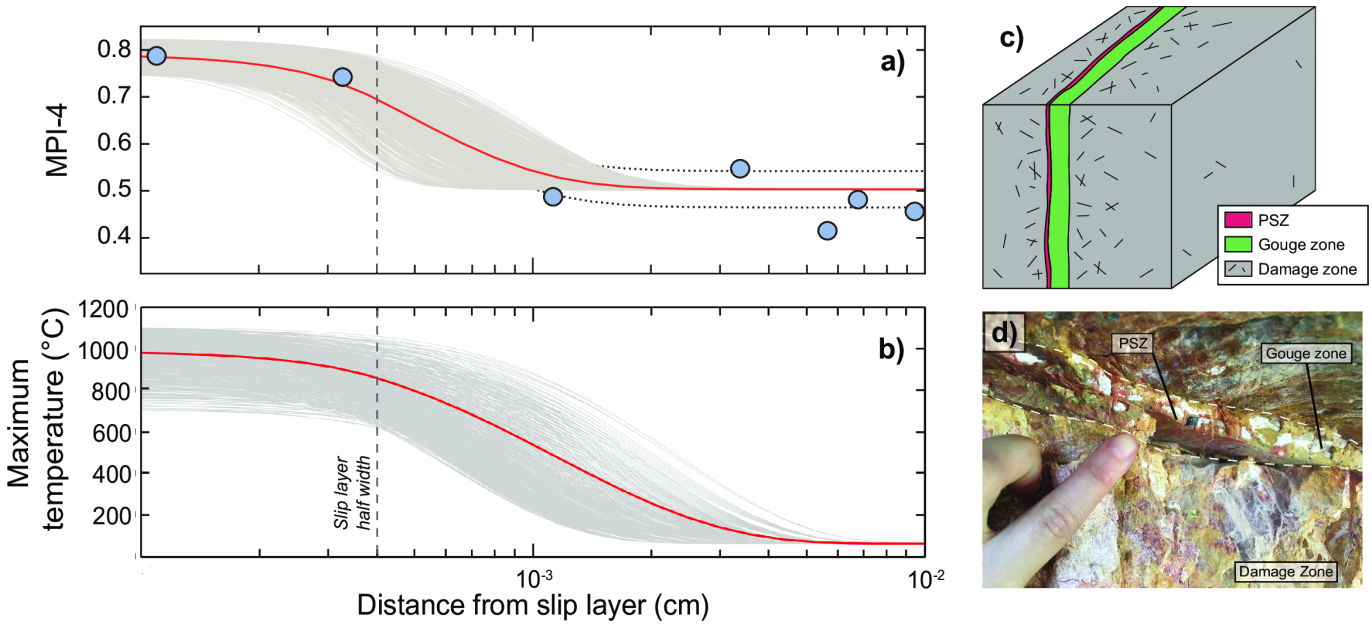

Figure 2 Examples of a) thermal maturity and b) maximum temperature from Coffey et al. (2019) as a function of the distance from the slipping layer. Profiles are modeled to fit measured biomarker (MPI-4) data shown by the blue points in a). Gray lines are 10,000 Monte Carlo iterations of the modeled thermal maturity and temperature profiles, and the red line is the mean. c) A simplified fault zone schematic showing the Principal Slip Zone (PSZ), gouge zone, and damage zone. d) photograph of a fault zone from the Muddy Mountain thrust in Nevada, USA.

such as the Nankai trough (Sakaguchi et al., 2011b). (U-Th)/He dating of hematite along fault surfaces has demonstrated that the thermal conditions occurring during earthquake slip are sufficient to reset U-Th/He ages along very localized surfaces (hundreds of μm thick) and that these reset ages can be used to model and constrain coseismic temperatures (Ault et al., 2015; McDermott et al., 2017; Ault et al., 2019; Armstrong et al., 2022).

In addition to these paleotemperature proxies, biomarkers have been increasingly used over recent years to investigate frictional heating, and they provide us with a robust and widely-applicable tool to explore coseismic temperature rise. Biomarkers are the molecular remains of past organisms that accumulate in sedimentary rocks over time. When heated, their abundance and molecular structure is systematically altered to achieve more thermally-stable configurations or products. This alteration can occur under earthquake temperatures and durations (Savage et al., 2018). While burial heating will also increase biomarker thermal maturity, comparing the difference in thermal maturity between fault zone and off-fault background samples reflects how much of the thermal maturity of the fault zone is due to temperature rise during the earthquake (Polissar et al., 2011; Savage et al., 2014; Savage and Polissar, 2019). Temperature can be calculated from biomarker thermal maturity because the kinetics for numerous biomarker reactions have been established from heating experiments (Sheppard et al., 2015; Rabinowitz et al., 2017). As a result, we can forward model temperature rise and biomarker reaction for a range of appropriate earthquake and fault parameters (Equation 1, Supplementary Material S1) to best fit the thermal maturity signal measured within a localized slip layer. For example, Figure 2 shows the best-fitting temperature model for one biomarker thermal maturity parameter, MPI-4 (methylphenanthrene index), for the Muddy Mountain thrust (Figure 2c). Biomarker thermal maturation is strongly temperature dependent, and larger events with the greatest temperature rise will dominate the maturity signal (Coffey et al., 2019). Because of this relationship and field observations of variability in displacement across different earthquakes on the same fault patch (Nicol et al., 2016), we assume that any biomarker heating signal present is a result of the largest earthquake the fault has experienced. As a result, estimates from biomarkers on the faults compiled here are likely upper bounds on temperature and frictional energy.

Three biomarker thermal maturity ratios are utilized in the dataset compiled here: the methylphenanthrene index (MPI-4) calculated from methylphenanthrene isomers (Coffey et al., 2019; Polissar et al., 2011; Savage et al., 2014), the Carbon Preference Index (CPI) calculated over C_{26}-C_{35} *n*-alkanes (Rabinowitz et al., 2017; Coffey et al., 2021; Rabinowitz et al., 2020), as well as the alkenone unsaturation ratio ($U^{k'}_{37}$) and concentrations from long-chain alkenones (Rabinowitz et al., 2017, 2020). More detailed information on the relevant thermal maturity parameters can be found in Supplementary Material S2.

Uncertainties in temperature estimates from biomarkers relate to uncertainties in the biomarker reaction kinetics, as well as the slip velocity, principal slip zone (PSZ) thickness, displacement, and shear stress during the event. The temperatures required for measurable biomarker reaction require seismic slip speeds, which limits the possible sliding velocity range (Savage et al., 2018). Slip zone thickness is measured

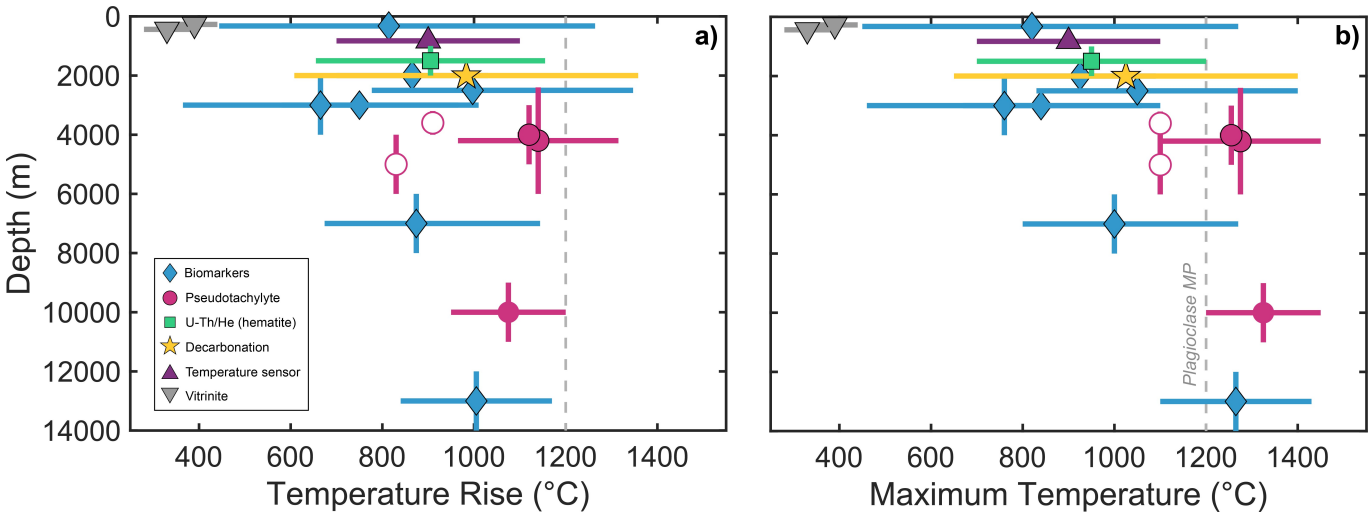

Figure 3 Compilation of earthquake temperatures with depth color-coded by proxy type. Symbols are mean and error bars are the 95% confidence intervals a) Earthquake temperature rise above background (i.e., does not include ambient temperature). b) Maximum temperature (temperature rise plus ambient temperature). Temperature rise during earthquakes is higher on more deeply buried faults because of increasing shear strength from increasing normal stress with depth. Open symbols are minimum bounds on temperature rise and maximum temperature.

in the field (Figure 2c); however, thickness may vary along a fault, and where possible we couple each temperature estimate with a measured thickness from the specific point along the fault that was sampled. Finally, although we typically do not know shear stress or displacement, we can place broad constraints on shear stress using in situ regional stress estimates and lab estimates of frictional weakening (e.g Collettini et al., 2009; Jeppson et al., 2010). Observational, experimental, and theoretical work of the last two decades has found that shear strength on large faults is most likely low during earthquake slip (Di Toro et al., 2011; Fulton et al., 2013; Rice et al., 2014). Simple models of earthquake slip based on Equation 1 (also in Equations 1 and 2 in Supplementary Material S1) demonstrate that if slip indeed localizes onto very thin layers as is often observed in the field (millimeter-scale or thinner; Figure 2c) and friction values were constant at ~0.6 as found in static friction experiments (e.g. Byerlee 1978), faults would reach unrealistically high temperature even during moderate earthquakes (Rice, 2006). High-velocity friction experiments confirmed that after a run-in phase of high friction, fault strength should drop dramatically for most rock types (Di Toro et al., 2011; Chang et al., 2012; Rubino et al., 2017). This drop in friction is a function of the thermal weakening displacement, D_{th} (Di Toro et al., 2011):

$$D_{th} = a\sigma_n^{-b} \tag{2}$$

where a and b are experimentally derived coefficients. As a result, the shear stress (τ) will evolve during sliding according to (Seyler et al., 2020):

$$\tau = \tau_{ss} + (\tau_p - \tau_{ss})e^{-\frac{\delta}{D_{th}}} \tag{3}$$

where τ_{SS} is the steady-state shear stress, τ_P is the peak shear stress, and δ is the slip accumulated after the peak shear stress. Because of this, the average shear stress during sliding will be lower for larger displacements as D_{th} is a lower fraction of total slip in these events, and more slip occurs at lower friction. In our models, we assume that shear stress evolves following Equation 3 and that normal stress is equal to overburden less hydrostatic pore pressure. We can then iterate the average friction as displacement increases and use this in our thermal models to define a shear stress range (Coffey et al., 2022).

3 Frictional Energy and the Earthquake Energy Budget

The energy expended during an earthquake is a function of the stress drop, $\Delta\sigma$, residual (dynamic) stress and total displacement, D, during the event. The available potential energy related to the stress drop due to the displacement, ΔW, is:

$$\Delta W = 1/2(\Delta\sigma D) \tag{4}$$

A simplified schematic of this is shown in Figure 1. Progress of the earthquake is delineated by the bold line and begins at some initial stress, σ_0. As the earthquake proceeds, stress drops to a final value, σ_f, over some displacement, D. During this time elastic strain energy in the volume around the slip surface is broadly converted into dissipative and radiated energy (Kanamori and Heaton, 2000). Radiated energy goes into the propagation of seismic waves, while dissipated energy includes fracture energy, which encompasses plastic deformation at the rupture tip and off-fault damage, as well as frictional energy, which is required to overcome frictional resistance (Kanamori and Brodsky, 2004; Kanamori and Rivera, 2006; Lambert et al., 2021; Viesca and Garagash, 2015).

Determining all components of the earthquake energy budget is difficult, as each component is estimated through different analyses. Radiated energy can in principle be determined from analysis of seismic waves.

The available energy, ΔW, depends on calculation of stress drop. The portion of the energy budget that is available energy less the radiated energy is often considered to go to fracture energy, but some of this energy can go to the dissipation of heat. As a result, some authors use the term breakdown energy as a more agnostic term because it is impossible to determine the amount of heat dissipation from seismological measurements (Cocco and Tinti, 2008; Lambert and Lapusta, 2020; Cocco et al., 2023). This distinction is important to note here because some of the temperature rise we measure could have in fact been part of the breakdown energy.

Coseismic temperature rise can be used to quantify the frictional energy dissipated during slip. We use the temperature proxies outlined above to identify seismic layers and quantify coseismic temperature rise. Frictional energy, E_F, is an integration of the product of velocity and shear stress, which is the total displacement during the earthquake, D:

$$E_F = \tau D \tag{5}$$

When referring to the frictional energy throughout the results of this study we are reporting frictional energy density (MJ/m^2) and emphasize that this will include any heat dissipated as part of the breakdown energy. Once the temperature rise, thickness of the fault, and the rock thermal and material properties have been established, the only unknown from Equation 1 is the product of the shear stress and displacement. We do not need to solve for shear stress and displacement to estimate temperature and frictional energy as their product is the important parameter. However, our estimate of shear stress from depth of faulting and frictional weakening across many rock types allows us to evaluate frictional energy as a function of displacement, and therefore earthquake size.

4 Thermal evidence of coseismic slip in faults

We compile estimates of coseismic temperature rise to synthesize what has been learned from investigations into coseismic temperature rise to date. We also compile estimates of frictional energy for the same faults where available, and for those faults where frictional energy has not been reported, we establish our own constraints based on our forward modeling described above. This compilation was made using a variety of thermal proxies, fault types, and tectonic settings and is presented in Table 1. New temperature estimates from biomarker thermal maturity are measured on the: Hundalee fault, Spoleto fault, Monte Maggio fault, and a thrust within the Marin Headlands (Supplementary Figure 1). We compare the temperature rise and frictional energy from these studies to fault and earthquake properties to explore any relationships that exist and the implications that some of these properties may have on earthquake rupture.

We estimate both absolute temperature and temperature rise (absolute temperature less the ambient temperature when independently calculated) during earthquake slip. We find that temperature rise ranges between 280 - 1350°C and the maximum temperature achieved by the fault ranges from ~280°C to 1450°C (Table 1; Figure 3). The lowest measurable temperatures (besides null results, which for the biomarker proxy depends on background thermal maturity but is usually less than ~500°C) were found in the Nankai frontal thrust using vitrinite reflectance (Sakaguchi et al., 2011b), while the highest temperatures occurred along the Pasagshak megathrust (Alaska) from biomarker measurements and the presence of pseudotachylyte (Rowe et al., 2005; Savage et al., 2014). The Pasagshak megathrust is unique in this dataset as it was exhumed from 12 - 14 km depth and has developed at least six pseudotachylyte layers, making it the deepest fault with the most evidence of frictional melt of the faults analyzed here.

We expect that fault strength increases with depth as a function of normal stress and frictional strength (Sibson, 1977; Byerlee, 1978), which would lead to an increase in both maximum temperature and temperature rise with increasing depth. Figure 3 demonstrates that both temperature rise and maximum temperature increase with depth down to ~5 km, below which temperature is more or less constant. This relationship between temperature and depth is apparent even though we are likely comparing earthquakes with different displacements (Supplementary Figure 2). Sibson and Toy (2006) showed a similar relationship between depth and temperature by demonstrating that pseudotachylyte is nearly absent in faults that were active at burial depths above ~3 km. If all other parameters except depth are held constant, a continued increase in temperature with depth is expected due to increasing normal stress and hence, shear strength. The observed nearly constant (or only subtly increasing) temperatures at depths below ~5 km may reflect that the faults in our database are mostly pseudotachylyte bearing at these depths. Once melting temperatures are achieved, melt lubrication may prevent further temperature rise (Ujiie et al., 2007; Kirkpatrick et al., 2012).

5 Earthquake Energy Budget

We combine frictional energy estimates from our biomarker studies with previous estimates from the literature and these are plotted in Figure 4. Frictional energy across all of the faults in this study varies from 0.9 – 228 MJ/m^2 (this range includes the 95% confidence interval limits of these estimates). This is generally higher than frictional energy estimates from laboratory experiments which range from 500 J/m^2 – 5 MJ/m^2 but involve displacements orders of magnitude lower than those considered in this compilation (Passelègue et al., 2016; Aubry et al., 2018; McBeck et al., 2019). The lowest frictional energy in our study occurs along faults of the frontal thrust of the Nankai subduction zone, which has a mean frictional energy of 2.5 MJ/m^2, (95% confidence interval: 0.9 – 3.8 MJ/m^2), while the highest occurs along the Pasagshak megathrust with a range of 105 – 228 MJ/m^2. The Pasagshak megathrust is a clear outlier,

Fault	PSZ thickness (mm)	Displacement (m)	Depth (m)	Burial T (°C)	Maximum T (°C)	T rise (°C)	Frictional energy (MJ/m^2)	Proxy	Source
Nankai megasplay	10	12.0 (7.7 - 19.9)	271	<20	340-440	340-440	16.2 (13.4 - 18.4)	Vitrinite reflectance	Sakaguchi et al. (2011a)
Papaku	0.1 - 2	11-15	300	10	820 (450-1270)	810 (440-1260)	8-13	Biomarkers	Saffer et al. (2019); Coffey et al. (2021)
Nankai frontal thrust	2	6.7 (1 - 19.1)	438	<20	280-380	280-380	6.5 (3.1 - 10.1)	Vitrinite reflectance	Sakaguchi et al. (2011b)
Japan trench	2.6-48	50	820-835	0	700-1100	700-1100	20-86	Biomarkers, borehole measurement	Brodsky et al. (2020); Fulton et al. (2013); Rabinowitz et al. (2020); Sun et al. (2017)
Wasatch damage zone	< 2	0.1-0.5	1000-2000	45	700-1200	650-1150	3.8 (2-7.4)	Hematite (U-Th)/He	Ault et al. (2015); McDermott et al. (2017)
Muddy Mountain	0.8 - 20	0.3-5	2000	60	760-1090	700-1030	6.7 (3.5-10.7)	Biomarkers	Brock and Engelder (1977); Coffey et al. (2019)
Monte Maggio	0.1 – 1	1.8 (0.1 -4.7)	2000	42	650-1400	508-1358	8.8 (1.6-18)	Biomarkers, carbonate decomposition	Collettini et al. (2014); Kaneko et al. (2016); Carpenter et al. (2014)
Spoleto	0.3 - 1	0.9 (0.06-2.0)	2000-3000	50	650-1300	600-1250	6.6 (1.2-10.6)	Biomarkers, decarbonation	Collettini et al. (2013)
Punchbowl	0.3 - 20	1-4	2000-4000	95	460-1060	365-955	2-25	Biomarkers	Chester et al. (2005); Savage and Polissar (2019)
Skeeter	0.25 – 10	1 (0.01-1.5)	2400-6000	110-160	1100-1450	940-1340	7.8 (2.5-11.7)	Pseudotachylyte	Kirkpatrick et al. (2012), this study
Central San Andreas	0.1 - 18	0.3-5	3000	90	840 (670-1100)	750 (580-1010)	8.2 (2.8-15.2)	Biomarkers	Coffey et al. (2022)
Nojima	1 – 3	2	3000-5000	110-160	1230-1280	1090-1140	17.4 (6.6-26.2)	Pseudotachylyte	Otsuki et al. (2003), this study
Marin Headlands	1 – 4	0.2 (0.1-0.5)	6000-8000	126	1000 (800-1270)	874 (674-1044)	6.3 (4.2-7.0)	Biomarkers	Regalla et al. (2018), this study
Hundalee	10 – 30	1.6 (0.9-2.2)	-	10	640 (500-900)	630 (490-890)	14.2 (1.3-19.7)	Biomarkers	Williams et al. (2018)
Larghe	6	0.3-2	9000-11000	250	1200-1450	950-1200	27 (22.8-32.9)	Pseudotachylyte	Di Toro and Pennacchioni (2005); Pittarello et al. (2008)
Pasagshak	30 - 50	1-8	12000-14000	260	1100-1430	840-1170	105-228	Biomarkers, Pseudotachylyte	Meneghini and Moore (2007); Rowe et al. (2011); Savage et al. (2014)
Shimanto[†] (Mugi)	>0.6-1.5	-	3200-4000	170-190	> 1100	>910-930	-	Pseudotachylyte	Ujiie et al. (2007)
Shimanto[†] (Okitsu)	>0.6-1.5	-	4000-6000	230-270	> 1100	>830-870	-	Pseudotachylyte	Ujiie et al. (2007)

Table 1 Thickness and number of PSZs observed as well as lithologies of each fault compiled here. Values reflect what was reported in the source for that data and are either a single value, which likely has considerable uncertainties, or a range that incorporates uncertainties. Values in brackets are 95% confidence intervals.

[†]Temperature and thickness data from Ujiie et al. (2007) for the two localities in the Shimanto accretionary complex are minimum bounds and no upper limit is given. We do not model displacement or frictional work here as a result of this uncertainty.

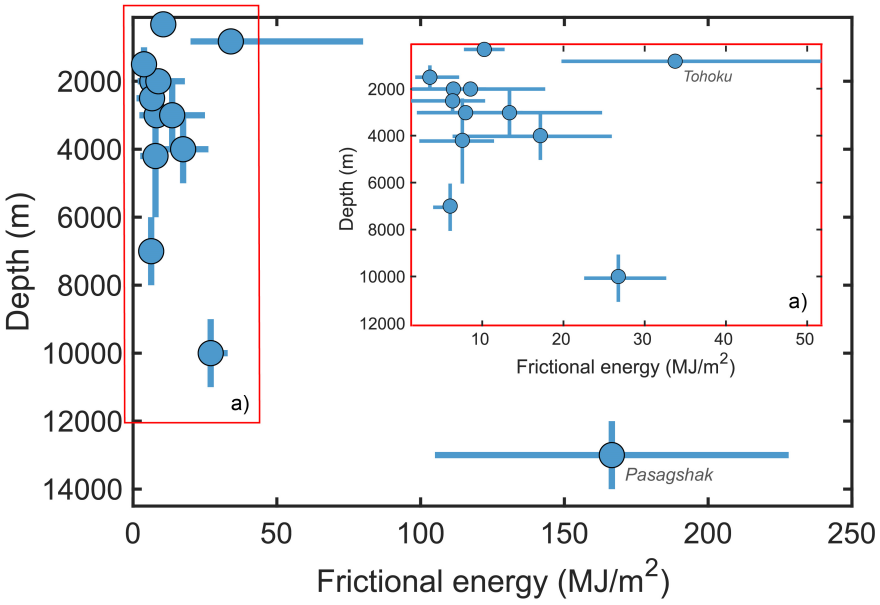

Figure 4 Depth plotted against frictional energy for faults in this compilation. Inset a), as outlined by the red box, shows frictional energy as a function of depth but only for those faults with a frictional energy ≤ 50 MJ/m^2. This only excludes the Pasagshak megathrust and highlights a slight trend in frictional energy at shallower depths (≤ ~5 km).

and as described above, it is unique in this dataset due to the thickness of pseudotachylyte that formed. The rest of the faults in this dataset have frictional energy that falls below 45 MJ/m^2, with most below 26 MJ/m^2, suggesting a tendency for frictional energy to remain within a narrow range despite differences in displacement, depth, fault type, lithology, or ambient temperature. While frictional energy varies over a relatively narrow range, we see a weak relationship between frictional energy and depth, similar to coseismic temperature rise, frictional energy increases slightly with depth until ~5 km (Figure 4). The exception to this trend is the Tohoku earthquake, where rapid fault zone drilling captured the temperature decay after that earthquake (Fulton et al., 2013).

By estimating the average shear stress during the earthquake (Equation 3), we can also estimate the earthquake displacement and compare frictional energy to values of fracture and radiated energy calculated from other studies. We used estimates from (Ye et al., 2016), which are included in their supplement. Radiated energy is estimated from the ground velocity spectra according to (Venkataraman and Kanamori, 2004). G', a proxy for fracture energy, which we refer to as breakdown energy, that is calculated as follows:

$$G' = 0.5(1 - \eta_R)\Delta\sigma_E D \quad (6)$$

where η_R is the radiation efficiency estimated from the ratio of measured radiated energy to available potential energy, $\Delta\sigma_E$ is the energy-related stress drop, and D is the average slip.

All components of the energy budget increase with displacement, however the frictional energy increase is subtle compared to the other components (Figure 5). Radiated energy is generally slightly lower than breakdown energy for a given displacement and can reach values of up to 20 MJ/m^2 when normalized by the rupture area. The breakdown energy on the other hand reaches values as large as 140 MJ/m^2 but generally falls below 100 MJ/m^2. Frictional energy (0.9 – 228 MJ/m^2) tends to locate toward the higher end of both the breakdown and radiated energy at a given displacement, although at high displacements frictional and breakdown energy become more similar.

The limited range of frictional energy values compared to breakdown and radiated energy may reflect a self-limiting process due to temperature-driven changes in fault strength. As sliding occurs at earthquake slip rates, friction evolves to a lower steady-state value over some thermal weakening distance, D_{th} (Di Toro et al., 2011; Paola et al., 2011). Accordingly, a large fraction of the total frictional energy should be released during the initial period of sliding before D_{th} is reached. Sliding after this distance dissipates little energy because the fault is weak, so that the total frictional energy increases only slightly for larger earthquakes (if at all). Weakening also explains the lack of relationship observed between frictional energy and depth for faults below~5 km (Figure 4), because D_{th} is smaller at higher normal stresses, and low friction is achieved with less total slip (Seyler et al., 2020). We acknowledge that fault weakening was assumed in our displacement estimates from biomarkers, however the consistency in frictional energy estimates in our field data require that frictional energy is not strongly dependent on displacement (e.g. if friction was at a constant level throughout the earthquake, frictional energy should increase linearly with displacement).

Using the values of breakdown, radiated, and frictional energy from Figure 5, we have put together a representative complete earthquake energy budget for small (<1-10 m of displacement) and large (>1-10 m of

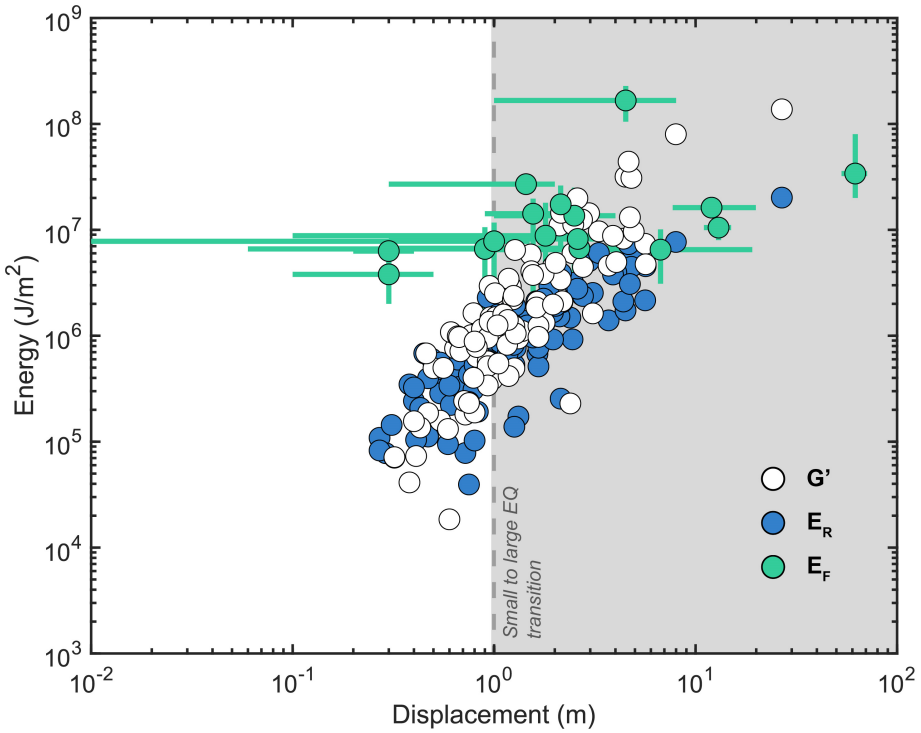

Figure 5 G' is breakdown energy and consists of fracture energy and some unknown component of frictional energy (Abercrombie and Rice, 2005), E_R is the radiated energy, and E_F is the frictional energy. E_R and G' are from Ye et al. (2016). E_F is compiled from previous studies or calculated here from temperature data (Table 1). Bars on frictional energy represent the range of displacement and E_F for each event. The dashed line and gray shaded region reflect the approximate transition from small (<1-10 m of displacement) to large earthquakes (>1-10 m of displacement)

displacement) events (Figure 6). The distinction at 1-10 m displacement, i.e., between small and large events, corresponds to the displacement where frictional energy is no longer the dominant energy sink (Figure 5). We suggest that as earthquakes get large and friction is low, a greater fraction of the total energy can go towards radiating seismic waves and towards deformation such as plastic deformation at the rupture tip and off-fault damage. Dedicating less energy to frictional resistance might allow earthquakes to keep propagating. Although our frictional energy dataset is small, it covers a range of depths, lithologies, fault thicknesses, and slip distances, suggesting that the basic relationships observed are fundamental and not the result of biases in the faults sampled. This observation of low friction at large displacements is what has been proposed from high velocity friction experiments and the efficacy of dynamic weakening mechanisms (Di Toro et al., 2011; Viesca and Garagash, 2015; Lambert et al., 2021), however the results from this study are the first that show this from field data. Our results provide insight into fundamental differences between small and large earthquakes, contributing to an integrated view of the earthquake energy budget and improving our overall understanding of how energy is partitioned during earthquakes.

6 Conclusions

Temperature rise and frictional energy have been compiled for newly analyzed and previously studied faults that reflect a range of different tectonic settings, depths, and earthquake sizes. This dataset has been used to better understand the role of frictional heating during earthquakes and place the first broad constraints on the total earthquake energy budget. Temperature rise increases with depth of faulting, which is likely a consequence of increasing normal stress. However, below ~5 km depth, temperature rise no longer increases, suggesting a temperature limit through thermal weakening mechanisms. While frictional energy increases somewhat with displacement, the increase is remarkably small across different faults, suggesting that dynamic weakening limits the frictional work along most faults to values below 45 MJ/m^2. Along with frictional energy estimates, we have aggregated radiated and breakdown energy estimates and created an integrated view of the earthquake energy budget as a whole. In doing this, we demonstrate a fundamental difference in the way energy is partitioned between small and large earthquakes. For small earthquakes, the energy budget is dominated by frictional energy, whereas for large earthquakes, frictional, breakdown, and radiated energy contribute more equally to the total budget as a consequence of rapid frictional strength reduction with accumulating slip. These findings are an important advancement in understanding the energy required for earthquake rupture.

Acknowledgements

Early versions of this manuscript were greatly improved by comments from Jamie Kirkpatrick, Thorne Lay,

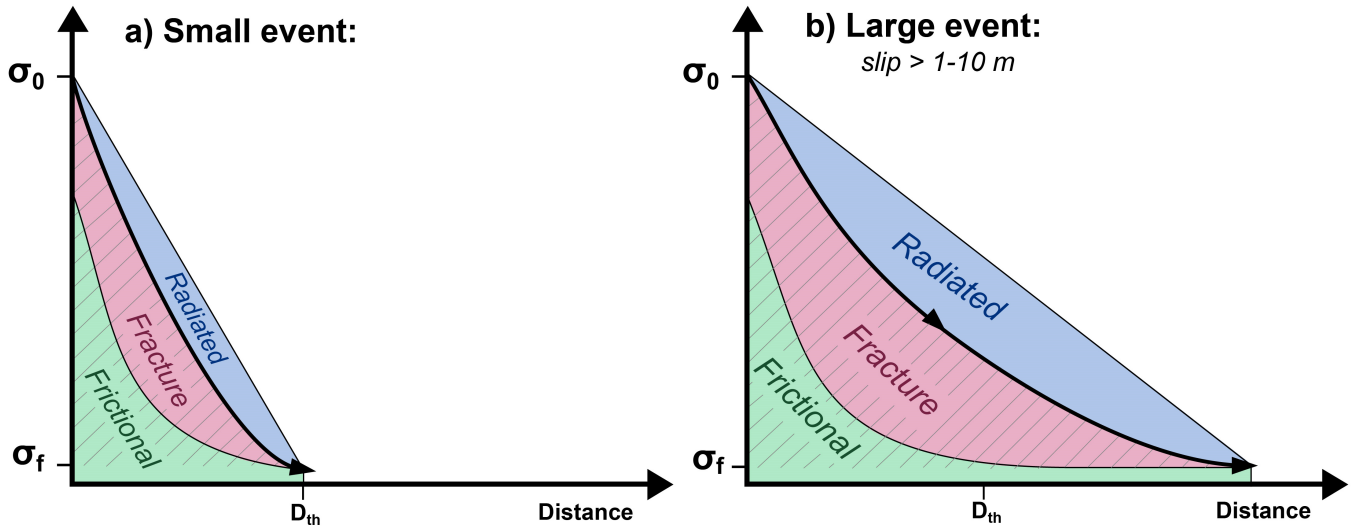

Figure 6 Schematic of the earthquake energy budget for small and large events with ranges for each component added. The bold line indicates stress drop as a function of slip and the colored areas represent the partitioning of energy into radiated (E_R), fracture (E_G), and frictional energy (E_F). The dashed region indicates the potential breakdown energy (G') and consists of fracture energy and some amount of frictional energy.

Christie Rowe, Rob Skarbek, and Nick Beeler. Conversations with Valere Lambert on earthquake energy budget helped us understand how best to compare different energy sinks and greatly improved the paper. Jack Williams graciously donated samples from the Hundalee fault. This work was partially supported by NSF Earthscope EAR1358585, DOE grant DE-SC0022360, and the Brinson Foundation (Chicago, IL). Heather Savage was partially supported by a UC Santa Cruz EVC Writing Felloship program. We thank Pathikrit Bhattacharya and an anonymous reviewer for the comments and suggestions, which improved the quality of this manuscript.

Data and code availability

Data used in this study can be found in the manuscript and supplementary material. Code for biomarker and thermal modelling can be found at 10.6084/m9.figshare.21308343

References

Abercrombie, R. and Rice, J. Can observations of earthquake scaling constrain slip weakening? *Geophysical Journal International*, 162(2):406–424, 2005. doi: 10.1111/j.1365-246X.2005.02579.x.

Armstrong, E., Ault, A., Bradbury, K., Savage, H., Polissar, P., and Thomson, S. A multi-proxy approach using zircon (U-Th)/he thermochronometry and biomarker thermal maturity to robustly capture earthquake temperature rise along the punchbowl fault, California. *Geochemistry, Geophysics, Geosystems*, 23(4), 2022. doi: 10.1029/2021gc010291.

Aubry, J., Passelègue, F., Deldicque, D., Girault, F., Marty, S., Lahfid, A., and Schubnel, A. Frictional heating processes and energy budget during laboratory earthquakes. *Geophysical Research Letters*, 45(22):12–274, 2018. doi: 10.1029/2018GL079263.

Ault, A., Reiners, P., Evans, J., and Thomson, S. Linking hematite (U-Th)/ He dating with the microtextural record of seismicity in the Wasatch fault damage zone. *Geology*, 43(9):771–774, 2015. doi: //doi.org/10.1130/G36897.1.

Ault, A., Jensen, J., Mcdermott, R., Shen, F., and Devener, B. Nanoscale evidence for temperature-induced transient rheology and postseismic fault healing. *Geology*, 48:1–5, 2019. doi: 10.1130/G46317.1.

Brock, W. and Engelder, T. Deformation associated with the movement of the Muddy Mountain overthrust in the Buffington window, southeastern Nevada. *Geological Society of America Bulletin*, 88:1667–1677, 1977.

Brodsky, E., Mori, J., Anderson, L., Chester, F., Conin, M., Dunham, E., Eguchi, N., Fulton, P., Hino, R., Hirose, T., and Others. The state of stress on the fault before, during, and after a major earthquake. *Annual Review of Earth and Planetary Sciences*, 48 (1):49–74, 2020. doi: 10.1146/annurev-earth-053018-060507.

Byerlee, J. Friction of Rocks. In Byerlee, J. and Wyss, M., editors, *Rock Friction and Earthquake Prediction*, page 615–626. Birkhäuser Basel, 1978. doi: 10.1007/978-3-0348-7182-2_4.

Carpenter, B., Scuderi, M., Collettini, C., and Marone, C. Frictional heterogeneities on carbonate-bearing normal faults: Insights from the Monte Maggio Fault, Italy. *Journal of Geophysical Research: Solid Earth*, 119(12):9062–9076, 2014. doi: 10.1002/2014JB011337.

Chang, J., Lockner, D., and Reches, Z. Rapid acceleration leads to rapid weakening in earthquake-like laboratory experiments. *Science*, 338(6103):101–105, 2012. doi: 10.1126/science.1221195.

Chester, J., Chester, F., and Kronenberg, A. Fracture surface energy of the Punchbowl fault, San Andreas system. *Nature*, 437(7055): 133–136, 2005. doi: 10.1038/nature03942.

Cocco, M. and Tinti, E. Scale dependence in the dynamics of earthquake propagation: Evidence from seismological and geological observations. *Earth and Planetary Science Letters*, 273(1-2): 123–131, 2008. doi: doi.org/10.1016/j.epsl.2008.06.025.

Cocco, M., Aretusini, S., Cornelio, C., Nielsen, S., Spagnuolo, E., Tinti, E., and Toro, G. Fracture Energy and Breakdown Work During Earthquakes. *Annual Review of Earth and Planetary Sciences*, 51, 2023. doi: 10.1146/annurev-earth-071822-100304.

Coffey, G., Savage, H., Polissar, P., Rowe, C., and Rabinowitz, H. Hot

on the trail: Coseismic heating on a localized structure along the Muddy Mountain fault, Nevada. *Journal of Structural Geology*, 120:67–79, 2019. doi: 10.1016/j.jsg.2018.12.012.

Coffey, G., Savage, H., Polissar, P., Meneghini, F., Ikari, M., Fagereng, A., Morgan, J., and Wang, M. Evidence of seismic slip on a large splay fault in the hikurangi subduction zone. *Geochemistry, Geophysics, Geosystems*, 22(8), 2021. doi: 10.1029/2021gc009638.

Coffey, G., Savage, H., Polissar, P., Cox, S., Hemming, S., Winckler, G., and Bradbury, K. History of earthquakes along the creeping section of the San Andreas fault. *Geology*, 50(4):516–521, 2022. doi: 10.1130/G49451.1.

Collettini, C., Niemeijer, A., Viti, C., and Marone, C. Fault zone fabric and fault weakness. *Nature*, 462(7275):907–910, 2009. doi: 10.1038/nature08585.

Collettini, C., Viti, C., Tesei, T., and Mollo, S. Thermal decomposition along natural carbonate faults during earthquakes. *Geology*, 41:927–930, 2013. doi: 10.1130/G34421.1.

Collettini, C., Carpenter, B., Viti, C., Cruciani, F., Mollo, S., and Tesei, T. Fault structure and slip localization in carbonate-bearing normal faults: An example from the Northern Apennines of Italy. *Journal of Structural Geology*, 67:154–166, 2014. doi: 10.1016/j.jsg.2014.07.017.

Di Toro, G. and Pennacchioni, G. Fault plane processes and mesoscopic structure of a strong-type seismogenic fault in tonalites, Adamello batholith, Southern Alps. *Tectonophysics*, 402(1-4 SPEC. ISS.):55–80, 2005. doi: 10.1016/j.tecto.2004.12.036.

Di Toro, G., Han, R., Hirose, T., Paola, N., Nielsen, S., Mizoguchi, K., Ferri, F., Cocco, M., and Shimamoto, T. Fault lubrication during earthquakes. *Nature*, 471(7339):494–498, 2011. doi: 10.1038/nature09838.

Fulton, P., Brodsky, E., Kano, Y., Mori, J., Chester, F., Ishikawa, T., Harris, R., Lin, W., Eguchi, N., and Toczko, S. Low Coseismic Friction on the Tohoku-Oki Fault Determined from Temperature Measurements. *Science*, 6153:1214–1217, 2013. doi: 10.1126/science.1243641.

Jeppson, T., Bradbury, K., and Evans, J. Geophysical properties within the San Andreas Fault Zone at the San Andreas Fault Observatory at Depth and their relationships to rock properties and fault zone structure. *Journal of Geophysical Research: Solid Earth*, 115(12):1–20, 2010. doi: 10.1029/2010JB007563.

Kanamori, H. and Brodsky, E. The physics of earthquakes. *Reports on Progress in Physics*, 67(8):1429–1496, 2004. doi: 10.1088/0034-4885/67/8/R03.

Kanamori, H. and Heaton, T. Microscopic and macroscopic physics of earthquakes. *Geophysical Monograph Series*, 120:147–163, 2000. doi: 10.1029/GM120.

Kanamori, H. and Rivera, L. Energy partitioning during an earthquake. *Geophysical Monograph Series*, 170:3–13, 2006. doi: 10.1029/170GM03.

Kaneko, Y., Nielsen, S., and Carpenter, B. The onset of laboratory earthquakes explained by nucleating rupture on a rate-and-state fault. *Journal of Geophysical Research: Solid Earth*, 121(8):6071–6091, 2016. doi: 10.1002/2016JB013143.

Kirkpatrick, J. and Rowe, C. Disappearing ink: How pseudotachylytes are lost from the rock record. *Journal of Structural Geology*, 52:183–198, 2013. doi: 10.1016/j.jsg.2013.03.003.

Kirkpatrick, J., Shipton, Z., and Persano, C. Pseudotachylytes: Rarely generated, rarely preserved, or rarely reported? *Bulletin of the Seismological Society of America*, 99(1):382–388, 2009. doi: 10.1785/0120080114.

Kirkpatrick, J., Dobson, K., Mark, D., Shipton, Z., Brodsky, E., and Stuart, F. The depth of pseudotachylyte formation from detailed thermochronology and constraints on coseismic stress drop variability. *Journal of Geophysical Research: Solid Earth*, 117(6):1–13, 2012. doi: 10.1029/2011JB008846.

Lachenbruch, A. Simple models for the estimation and measurement of frictional heating by an earthquake, 1986.

Lambert, V. and Lapusta, N. Rupture-dependent breakdown energy in fault models with thermo-hydro-mechanical processes. *Solid Earth*, 11(6):2283–2302, 2020. doi: 10.5194/se-11-2283-2020.

Lambert, V., Lapusta, N., and Perry, S. Propagation of large earthquakes as self-healing pulses or mild cracks. *Nature*, 591(7849): 252–258, 2021. doi: 10.1038/s41586-021-03248-1.

McBeck, J., Cordonnier, B., Mair, K., and Renard, F. The evolving energy budget of experimental faults within continental crust: Insights from in situ dynamic X-ray microtomography. *Journal of Structural Geology*, 123:42–53, 2019. doi: 10.1016/j.jsg.2019.03.005.

McDermott, R., Ault, A., Evans, J., and Reiners, P. Thermochronometric and textural evidence for seismicity via asperity flash heating on exhumed hematite fault mirrors, Wasatch fault zone, UT, USA. *Earth and Planetary Science Letters*, 471:85–93, 2017. doi: 10.1016/j.epsl.2017.04.020.

Meneghini, F. and Moore, J. Deformation and hydrofracture in a subduction thrust at seismogenic depths: The Rodeo Cove thrust zone, Marin Headlands, California. *Bulletin of the Geological Society of America*, 119(1-2):174–183, 2007. doi: 10.1130/B25807.1.

Nicol, A., Robinson, R., Dissen, R., and Harvison, A. Variability of recurrence interval and single-event slip for surface-rupturing earthquakes in New Zealand. *New Zealand Journal of Geology and Geophysics*, 59(1):97–116, 2016. doi: 10.1080/00288306.2015.1127822.

Noda, H. and Lapusta, N. Stable creeping fault segments can become destructive as a result of dynamic weakening. *Nature*, 493 (7433):518–521, 2013. doi: 10.1038/nature11703.

Otsuki, K., Monzawa, N., and Nagase, T. Fluidization and melting of fault gouge during seismic slip: Identification in the Nojima fault zone and implications for focal earthquake mechanisms. *Journal of Geophysical Research: Solid Earth*, 108(B4), 2003. doi: 10.1029/2001JB001711.

Paola, N., Hirose, T., Mitchell, T., Toro, G., Viti, C., Shimamoto, T., and Laterina, V. Fault lubrication and earthquake propagation in thermally unstable rocks. *Geology*, 39(1):35–38, 2011. doi: 10.1130/G31398.1.

Passelègue, F., Schubnel, A., Nielsen, S., Bhat, H., Deldicque, D., and Madariaga, R. Dynamic rupture processes inferred from laboratory microearthquakes. *Journal of Geophysical Research: Solid Earth*, 121(6):4343–4365, 2016. doi: 10.1002/2015JB012694.

Pittarello, L., Di Toro, G., Bizzarri, A., Pennacchioni, G., Hadizadeh, J., and Cocco, M. Energy partitioning during seismic slip in pseudotachylyte-bearing faults, Gole Larghe Fault, Adamello, Italy. *Earth and Planetary Science Letters*, 269(1-2):131–139, 2008. doi: 10.1016/j.epsl.2008.01.052.

Polissar, P., Savage, H., and Brodsky, E. Extractable organic material in fault zones as a tool to investigate frictional stress. *Earth and Planetary Science Letters*, 311(3-4):439–447, 2011. doi: 10.1016/j.epsl.2011.09.004.

Rabinowitz, H., Polissar, P., and Savage, H. Reaction kinetics of alkenone and n-alkane thermal alteration at seismic timescales. *Geochemistry, Geophysics, Geosystems*, 18(1):204–219, 2017. doi: 10.1002/2016GC006553.

Rabinowitz, H., Kirkpatrick, J., Savage, H., Polissar, P., and Rowe, C. Earthquake slip surfaces identified by biomarker thermal matu-

rity within the 2011 Tohoku-Oki earthquake fault zone. *Nature Communications*, 11(533):1–9, 2020. doi: 10.1038/s41467-020-14447-1.

Reches, Z. and Lockner, D. Fault weakening and earthquake instability by powder lubrication. *Nature*, 467(7314):452–455, 2010. doi: 10.1038/nature09348.

Regalla, C., Rowe, C., Harrichhausen, N., Tarling, M., and Singh, J. Styles of underplating in the Marin Headlands terrane, Franciscan complex, California. *Special paper of the Geological Society of America*, 534:155–173, 2018. doi: 10.1130/2018.2534(10).

Rice, J. Heating and weakening of faults during earthquake slip. *Journal of Geophysical Research*, 111:1–29, 2006. doi: 10.1029/2005JB004006.

Rice, J., Rudnicki, J., and Platt, J. Stability and localization of rapid shear in fluid-saturated fault gouge: 1. Linearized stability analysis. *Journal of Geophysical Research: Solid Earth*, 119 (5):4311–4333, 2014. doi: 10.1002/2013JB010710.

Rodriguez-Navarro, C., Ruiz-Agudo, E., Luque, A., Rodriguez-Navarro, A., and Ortega-Huertas, M. Thermal decomposition of calcite: Mechanisms of formation and textural evolution of CaO nanocrystals. *The American Mineralogist*, 94(4):578–593, 2009. doi: 10.2138/am.2009.3021.

Rowe, C. and Griffith, W. Do faults preserve a record of seismic slip: A second opinion. *Journal of Structural Geology*, 78:1–26, 2015. doi: 10.1016/j.jsg.2015.06.006.

Rowe, C., Moore, J., Meneghini, F., and McKeirnan, A. Large-scale pseudotachylytes and fluidized cataclasites from an ancient subduction thrust fault. *Geology*, 33(12):937–940, 2005. doi: 10.1130/G21856.1.

Rowe, C., Meneghini, F., and Casey Moore, J. Textural record of the seismic cycle: Strain-rate variation in an ancient subduction thrust. *Geological Society Special Publication*, 359(1):77–95, 2011. doi: 10.1144/SP359.5.

Rubino, V., Rosakis, A., and Lapusta, N. Understanding dynamic friction through spontaneously evolving laboratory earthquakes. *Nature Communications*, 8:15991, 2017. doi: 10.1038/ncomms15991.

Saffer, D., Wallace, L., Barnes, P., Pecher, I., Petronotis, K., Levay, L., Bell, R., Crundwell, M., Fagereng, A., Fulton, P., Greve, A., Harris, R., Hashimoto, Y., Ikari, M., Ito, Y., Kitajima, H., Kutterolf, S., Lee, H., Li, X., and Wang, X. Site U1518. In *Proceedings of the International Ocean Discovery Program*, volume 372B/375, page 1–63, 2019. doi: 10.14379/iodp.proc.372B375.101.2019.

Sakaguchi, A., Chester, F., Curewitz, D., Fabbri, O., Goldsby, D., Kimura, G., Li, C., Masaki, Y., Screaton, E., Tsutsumi, A., Ujiie, K., and Yamaguchi, A. Seismic slip propagation to the up-dip end of plate boundary subduction interface faults: Vitrinite reflectance geothermometry on integrated ocean drilling program nantro SEIZE cores. *Geology*, 39(4):395–398, 2011a. doi: 10.1130/G31642.1.

Sakaguchi, A., Kimura, G., Strasser, M., Screaton, E., Curewitz, D., and Murayama, M. Episodic seafloor mud brecciation due to great subduction zone earthquakes. *Geology*, 39(10):919–922, 2011b. doi: 10.1130/G32043.1.

Savage, H. and Polissar, P. Biomarker Thermal Maturity Reveals Localized Temperature Rise from Paleoseismic Slip along the Punchbowl Fault, CA, USA. *Geochemistry, Geophysics, Geosystems*, 20:3201–3215, 2019. doi: 10.1029/2019GC008225.

Savage, H., Polissar, P., Sheppard, R., Rowe, C., and Brodsky, E. Biomarkers heat up during earthquakes: New evidence of seismic slip in the rock record. *Geology*, 42(2):99–102, 2014. doi: 10.1130/G34901.1.

Savage, H., Rabinowitz, H., Spagnuolo, E., Aretusini, S., Polissar, P., and Di, G. Biomarker thermal maturity experiments at earthquake slip rates. *Earth and Planetary Science Letters*, 502: 253–261, 2018. doi: 10.1016/j.epsl.2018.08.038.

Seyler, C., Kirkpatrick, J., Savage, H., Hirose, T., and Faulkner, D. Rupture to the trench? Frictional properties and fracture energy of incoming sediments at the Cascadia subduction zone. *Earth and Planetary Science Letters*, 546:116413, 2020. doi: 10.1016/j.epsl.2020.116413.

Sheppard, R., Polissar, P., and Savage, H. Organic thermal maturity as a proxy for frictional fault heating: Experimental constraints on methylphenanthrene kinetics at earthquake timescales. *Geochimica et Cosmochimica Acta*, 151:103–116, 2015. doi: 10.1016/j.gca.2014.11.020.

Sibson, R. Interactions between Temperature and Pore-Fluid Pressure during Earthquake Faulting and a Mechanism for Partial or Total Stress Relief. *Nature*, 243:66–68, 1973. doi: 10.1038/physci243066a0.

Sibson, R. Generation of Pseudotachylyte by Ancient Seismic Faulting. *Geophysical Journal of the Royal Astronomical Society*, 43:775–794, 1975. doi: 10.1111/j.1365-246X.1975.tb06195.x.

Sibson, R. Fault rocks and fault mechanisms. *Journal of the Geological Society*, 133(3):191–213, 1977. doi: 10.1144/gsjgs.133.3.0191.

Sibson, R. and Toy, V. The habitat of fault-generated pseudotachylyte: Presence vs. absence of friction-melt. *Geophysical Monograph Series*, 170:153–166, 2006. doi: 10.1029/170GM16.

Sun, T., Wang, K., Fujiwara, T., Kodaira, S., and He, J. Large fault slip peaking at trench in the 2011 Tohoku-oki earthquake. *Nature Communications*, 8:4–11, 2017. doi: 10.1038/ncomms14044.

Ujiie, K., Yamaguchi, H., Sakaguchi, A., and Toh, S. Pseudotachylytes in an ancient accretionary complex and implications for melt lubrication during subduction zone earthquakes. *Journal of Structural Geology*, 29(4):599–613, 2007. doi: 10.1016/j.jsg.2006.10.012.

Venkataraman, A. and Kanamori, H. Observational constraints on the fracture energy of subduction zone earthquakes. *Journal of Geophysical Research: Solid Earth*, 109:1–20, 2004. doi: 10.1029/2003JB002549.

Viesca, R. and Garagash, D. Ubiquitous weakening of faults due to thermal pressurization. *Nature Geoscience*, 8(11):875–879, 2015. doi: 10.1038/ngeo2554.

Williams, J., Barrell, D., Stirling, M., Sauer, K., Duke, G., and Hao, K. Surface rupture of the Hundalee fault during the 2016 Mw 7.8 Kaikōura earthquake. *Bulletin of the Seismological Society of America*, 108(3B):1540–1555, 2018. doi: 10.1785/0120170291.

Ye, L., Lay, T., Kanamori, H., and Rivera, L. Rupture characteristics of major and great (Mw≥7.0) megathrust earthquakes from 1990 - 2015: 1. Source parameter scaling relationships. *Journal of Geophysical Research: Solid Earth*, 121:3782–3803, 2016. doi: 10.1002/2015JB012426.